Marine Geology 469 (2024) 107246

Contents lists available at ScienceDirect

Marine Geology

journal homepage: www.elsevier.com/locate/margo

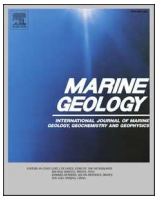

Pacific seafloor in the 40–52 Myr old portion of the Molokai to Murray corridor

Donna K. Blackman [a,*], Sujania Talavera-Soza [b], Ruei-Jiun Hung [b,c], John A. Collins [d], Gabi Laske [b]

[a] Department of Earth & Planetary Sciences, University of California, Santa Cruz, USA
[b] Inst. Geophysics & Planetary Physics, Scripps Institution of Oceanography, University of California, San Diego, USA
[c] Department of Earth and Environmental Sciences, San Diego State University, San Diego, USA
[d] Department of Geology & Geophysics, Woods Hole Oceanographic Institution, United States of America

ARTICLE INFO

Keywords:
Seamounts
NE Pacific
Geophysics

ABSTRACT

A detailed study of the character of 40–52 Myr old Northeast Pacific seafloor illustrates how volcanism that occurs outside a spreading center axial zone contributes to the morphology of a region. A compilation of new and pre-existing multibeam sonar data forms the basis of our study, which lies within the spreading corridor bounded by Molokai and Murray fracture zones and does not include a major volcanic chain. The broad structure is consistent with constant crustal thickness and lithospheric cooling with age, and our analyses focus on the deviations from this 'reference' model. We find three types of volcanic features where typical abyssal hill fabric is generally not observed: 1) volcanic ridges that have a length of 30–120 km and a height of 1–2 km; 2) moderate seamounts that have a diameter of 8–15 km and a height of several 100's m; and 3) fields of very small seamounts, which extend several 10's km and are more common at ~25% coverage than in other Pacific regions away from major volcanic chains. Gravity analysis suggests that the volcanic ridges and a few of the moderate seamounts are associated with local crustal thickening whereas the fields of very small seamounts do not display a distinct mass anomaly. Quantifying the distribution of past volcanism in this section of the Pacific plate during its evolution after initial accretion helps illustrate the degree of off-axis magmatism. Although we interpret the volcanic ridges as presently inactive, their formation on lithosphere older than at least a few Myr likely had an impact on the local seismic structure.

1. Introduction

Characterization of the seafloor on a portion of 40–52 Myr old Pacific lithosphere between the Molokai and Murray Fracture Zones (FZs) provides new insight into its structure and evolution. Accretion of oceanic crust involves continual interplay between magma supply from the mantle and crustal faulting due to tectonic forces that drive plate spreading. On geologic time scales, the waxing and waning of these respective factors results in fairly constant seafloor morphology and crustal structure along fast-spreading centers (Macdonald, 1982; Sinton and Detrick, 1992). A volcanic carapace averaging ~1.5 km thick overlies a ~ 4.5 km thick plutonic lower crust which, in turn, overlies denser peridotite mantle that extends to depth. Abyssal hills are formed via offset on spreading-center-parallel normal faults which are active within/near the rift axis and spaced a few km apart. The back-tilted abyssal hill blocks are composed of volcanic rock and have relief of 100's m. Occasional small seamounts occur if some magma from the subaxial mantle upwelling zone is not confined to the spreading axis (Batiza, 1982; Alexander and Macdonald, 1996; Shen et al., 1993; White et al., 1998; Briais et al., 2009). This basic structure drifts off-axis and the seafloor deepens, as the mantle portion of the lithosphere cools and its density increases, in proportion to the square root of plate age (Parsons and Sclater, 1977). The aim of this paper is to explore where the present day seafloor morphology in our study area deviates from this basic structure, to infer what processes could be involved, and to provide a framework for forthcoming seismic analyses that can determine whether subseafloor structure indicates ongoing mantle activity.

Our study area comprises crust formed along an eastern Pacific spreading center that was offset to the north and south by large transform faults, now traced by the Molokai and Murray FZ (Fig. 1).

* Corresponding author.
E-mail address: dkblackm@ucsc.edu (D.K. Blackman).

https://doi.org/10.1016/j.margeo.2024.107246
Received 14 August 2023; Received in revised form 12 February 2024; Accepted 16 February 2024
Available online 18 February 2024

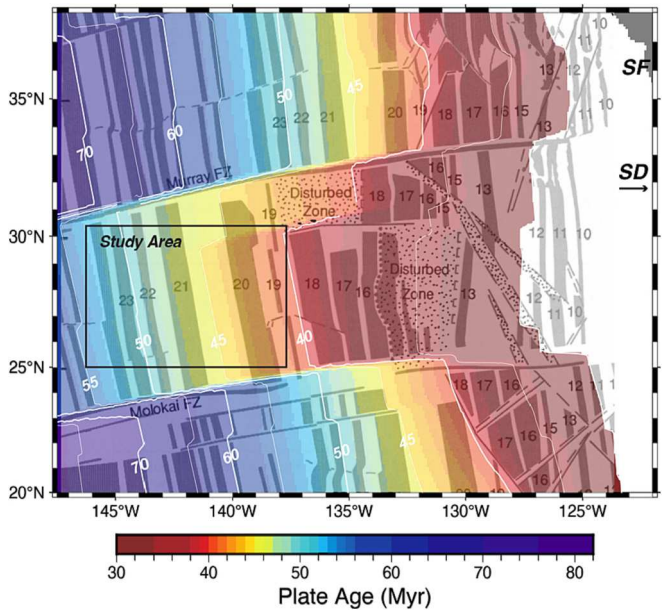

Fig. 1. Age of eastern central Pacific crust (Seton et al., 2020; color with white contours every 5 Myr), magnetic anomalies (gray stripes, anomaly number labeled), fracture zones, and deformation zones (stippled) identified by Atwater (1989) and modeled by Harrison and Sclater (1972). SF locates San Francisco; SD points toward San Diego.

Compilation of new and pre-existing multi-beam bathymetry data in the ~500 × 600 km area, results in fairly complete and detailed coverage, which allows us to systematically map abyssal hill orientation, large volcanic ridges, and fields of small seamounts. Gravity analysis guides our initial assessment of the subsurface structure and genesis of these features.

An array of Ocean Bottom Seismometers (OBS) was deployed across the study area in November–December 2022 and recovered January–February 2023 (Laske et al., 2023). Tracklines between the OBS stations were designed to maximize new seafloor mapping to the extent time allowed. The compiled dataset represents a significant addition to high-resolution (200 m) Pacific seafloor mapping, covering 300,000 km^2. In addition to portraying the post-accretion magmatic activity that influenced the morphology of the seafloor, our detailed description and provision of openly available data also supports our seismic analyses and can augment future studies of Pacific tectonics and underlying mantle processes.

2. Regional setting

The crust in our study area formed 40–52 Ma along a ~ 700 km section of the East Pacific Rise (EPR). Subsequently, the EPR ceased spreading 12–13 Ma and approached subduction beneath North America (Atwater, 1989). The half-rate of spreading ranged from ~59–73 km/Myr along the main spreading segment, with a fairly rapid increase from lower to higher rate ~ 48 Ma (Seton et al., 2020). A single ridge segment produced crust throughout much of the study area (Fig. 1). However, secondary segmentation has occurred in this spreading corridor, as evidenced by offsets in magnetic anomaly patterns and derived isochrons (Atwater, 1989; Seton et al., 2020). A southern segment extending ~330 km N from the Molokai FZ was offset 30 km W of the main segment until ~50 Ma when the offset began to shrink to elimination. In the north, an offset developed ~48 Ma and its length grew steadily to ~250 km by 40 Ma. This northern segment extends S from the Murray FZ for ~200 km and created crust on the W flank at ~110 km/Myr. At 40 Ma, another offset developed and reached ~80 km length over the next 5 Myr, separating a segment ~100 km long to the S of the northern segment. An eastward ridge jump, and asymmetric spreading were likely involved in the segmentation evolution. Harrison and Sclater (1972) conclude that a ridge jump occurred ~40 Ma, creating crust that is presently just outside the study area to the east.

The corridor between the Molokai and Murray FZs is unusual for how far offset the spreading axis was from the main trend of the EPR in this region, forming a 'tooth' that juts out 580 km to the west. Mantle upwelling zones, where partial melting that provides a supply of magma to form new ocean crust occurs, are expected to be on the order of 100 km wide beneath the northern EPR (Key et al., 2013; Sparks and Parmentier, 1992; Wang et al., 2009). Thus, this is an interesting case where 3-D asthenospheric conditions (temperature, dynamic flow stresses) and increased lithospheric stresses (Fox and Gallo, 1984), both associated with the large segment offset and contrast in lithospheric thickness across the ridge-transform intersections, could potentially influence the isolated spreading center's behavior.

An additional factor in the tectonic evolution of the corridor may be far-field stresses due to the impingement of the Pacific plate on North and Central America (Atwater, 1989). Such rigid deformation becomes prominent farther east (Fig. 1), as evidenced by propagating rift scars, disturbance of the typical abyssal hill seafloor fabric, and rotation of plate fragments.

3. Bathymetry in the study area

3.1. Data acquisition and processing

All multi-beam bathymetry (MB) data in the study area that was archived as of January 2023 at the U.S. National Centers for Environmental Information (NCEI, https://www.ncei.noaa.gov/maps/bathymetry/) were downloaded and checked for data quality. Data from 23 of the 34 prior cruises that we used (Fig. 2a) required further editing to remove noisy pings and outlier values (Table S1). Navigation was not adjusted using bathymetric matching at crossings since GPS was available for each prior cruise included and mismatch on overlapping swaths was not an issue at the scale of our study. Data acquired during our OBS deployment cruise aboard *R/V Kilo Moana* (KM2117) and the recovery cruise aboard *R/V Sally Ride* (SR2302) were also edited using MBSystem *mbedit* and then the full set of data was gridded using *mbgrid*. Ship speed was generally ~10 kts, so no ping averaging was done for the creation of our 200 m bathymetry grid of the full area (Fig. 2b).

Deepening of the seafloor with age is a dominant, and expected, signal in the bathymetric map. Since plate-cooling is well known and models of deepening as an exponential function of the age has been shown to fit a majority of Earth's ocean floor >20 Myr old (Stein and Stein, 1992), we removed this component: $z_{deepen} = 5651–2473 \times \exp.(-0.0278 \times \text{age (Myr)})$ m. We used the plate age model of Seton et al. (2020) with the Gee and Kent (2007) timescale in this calculation. The resulting 'residual bathymetry' map (Fig. 3) is the basis of our analysis of seafloor features.

3.2. Seafloor features

Abyssal hills are prominent in ~60% of the study area and their orientation parallels the isochrons in all but about 15% of this seafloor (Fig. 3). Subareas where the abyssal hill orientation deviates by >4° from isochron-parallel were determined by systematically comparing local trend with the regional, isochron-parallel direction. The observed trend deviation was marked and labeled at each such location. Almost all of the western 2/3 of the study area has abyssal hill orientations that are isochron-parallel. Much of the northeast corner of the study area has abyssal hill orientations that deviate 16–25° clockwise from the isochrons. A portion of the southeastern corner has abyssal hill deviations that are generally 14° counter-clockwise from isochron-parallel.

Features that are 1–2 km shallower than adjacent seafloor and extend roughly linearly for 30–120 km are defined as volcanic ridges

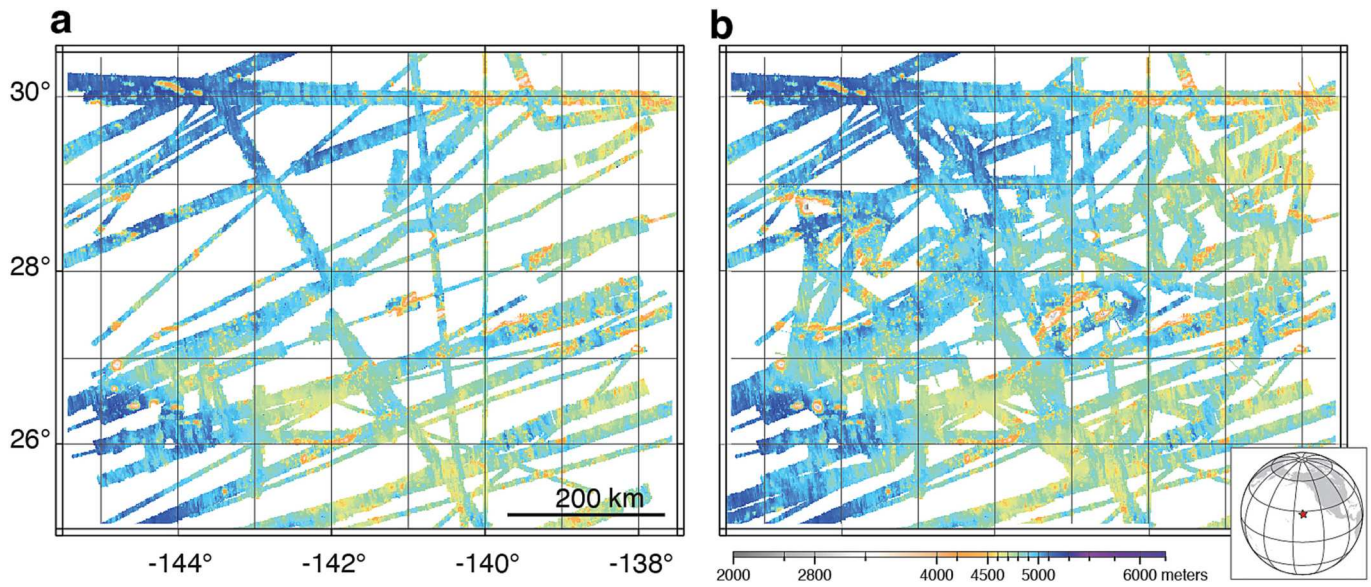

Fig. 2. Multibeam sonar data in the study area (a) prior to our mapping and (b) after.

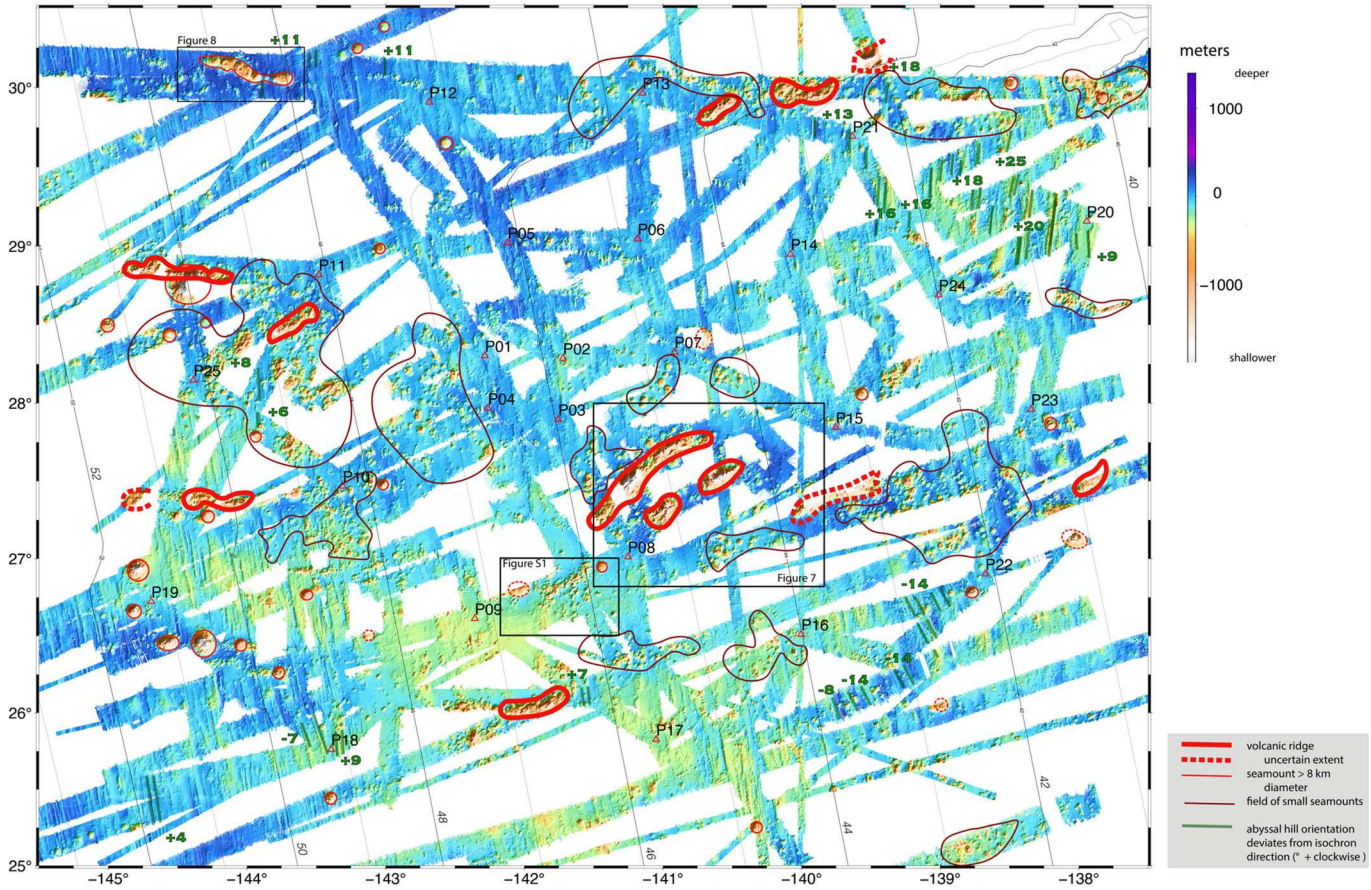

Fig. 3. *(below)*. Residual bathymetry map shows deviation from deepening with age. Features that differ from the typical abyssal hills and their expected trend are identified (legend lower right). Thin black lines are isochrons (age indicated in Myr). OBS locations are shown by red triangles and labeled with station name. Subsequent figure locations are identified (boxes).

(VR, Fig. 3). These occur on about 3% of the seafloor in the study area, and their morphology is typical of volcanic structures groundtruthed elsewhere by direct seafloor observation/sampling. The trends of the VR are neither spreading-parallel (isochron perpendicular) nor isochron-parallel, although about half trend ~EW and are much closer to the former than the latter. The rest of the VR trend ~30° S of spreading-parallel.

Moderate seamounts are defined here as mainly circular features having diameter 8 km or greater (Fig. 3). Several of these are flat-topped, with heights typically 600–1000 m. Craters and/or small

cones are visible on their tops in many cases. Moderate seamounts that are not flat-topped typically have heights greater than a kilometer above surrounding seafloor. Altogether, moderate seamounts comprise about 2% of the study area. Most of the moderate seamounts occur away from volcanic ridges and fields of small seamounts. One line of moderate seamounts in the NW (~30°N, 144°W) extends in a trend that is similar to the trend of several volcanic ridges (Fig. 3).

Fields of very small seamounts (diameter < 6 km, height < 500 m) occur in various sizes, ranging from ~30 to 150 km in extent (Fig. 3). The choice of where to draw the boundary of such fields is somewhat subjective and gaps in coverage add to the uncertainty. Visual inspection of where the density of small, clearly volcanic features was greater than average determined our choice of boundary lines. These fields of small seamounts usually do not display abyssal hill morphology. Combined, these fields cover around 25% of the study area. Many of the fields of small seamounts are between latitudes 27°N and 29°N but several also occur outside this band.

An area with distinct morphology occurs just to the south of the center of the study area (26°35′-27°N, 142°-141°30′W, Fig. 3 and enlarged view in Fig. S1). The volcanic features (Fig. S1) distributed throughout this area are similar in size to the very small seamounts but, rather than being circular, they form 2–4 km long ridges up to 600 m in height. The ridge tops are narrow, and the shoulders taper toward background seafloor depths, sometimes in multiple directions that are reminiscent of branch rift zones on subaerial volcanoes. Two moderate seamounts bookend the northern edges of this area.

3.3. Comparison to satellite-Derived Bathymetry Model

The Smith and Sandwell (1997, updated version SRTM15_V2.4) global bathymetry model based on satellite gravity provides a good representation of the seafloor where MB track data are included. Fig. 4 shows that such areas generally agree with our 200-m gridded MB data to within ~25 m. Portions of some MB tracks included in the model grid have greater misfit at the edges, where further editing was done to remove edge noise, as the southeastern-most track segment in the study area illustrates. As expected, our new MB data show significantly more detail than the portion of the model constrained only by satellite-based estimates. At multi-km wavelengths that are within the resolution of the satellite-based model, the largest volcanoes in our study area (diameter on the order of 20 km) show the greatest mismatch, with an overshoot effect causing peaks to be too shallow in the model, and to be surrounded by 'moats' that are too deep. The magnitude of misfits around these features can exceed 500 m. Even the line of moderate seamounts in the NW show this effect. Actual seamounts of 10–20 km diameter are more steeply sided and have less conical peaks than the model portrays.

Occasional small-scale artifacts show up in the comparison of the global bathymetry model and the MB-based 200 m grid. Latitude-parallel striping is evident along many portions of the 30°N latitude trackline (Fig. 4). It is also visible along a 26°N latitude trackline in the central longitudes (142°30′-143°40′W) as well as eastern portions of the NE-trending tracks that exit the study area between 27° and 28°N. Typically, these 'stripes' are positive (global model deeper than our 200 m grid) but in some places there is an adjacent negative stripe. Just a few places show a short section of longitude-parallel striping as well. To obtain the difference map the SRTM15_V2.4 grid was subsampled using bicubic interpolation with GMT grdsample (Wessel et al., 2019) and then subtracted from our 200 m grid. This should not introduce the artifacts that are seen. They only occur in a few locations, and only along pre-existing tracks included in the SRTM15_V2.4 grid; their magnitude can reach 200–300 m.

4. Lateral density variations

Gravity data can indicate whether mass anomalies are associated with any of the anomalous bathymetric features described in the last section or related to segmentation within the corridor. Determined relationships, or lack thereof, may suggest the process(es) responsible for the formation of the observed seafloor features. We use a well-established method to remove from the Free Air Anomaly map the

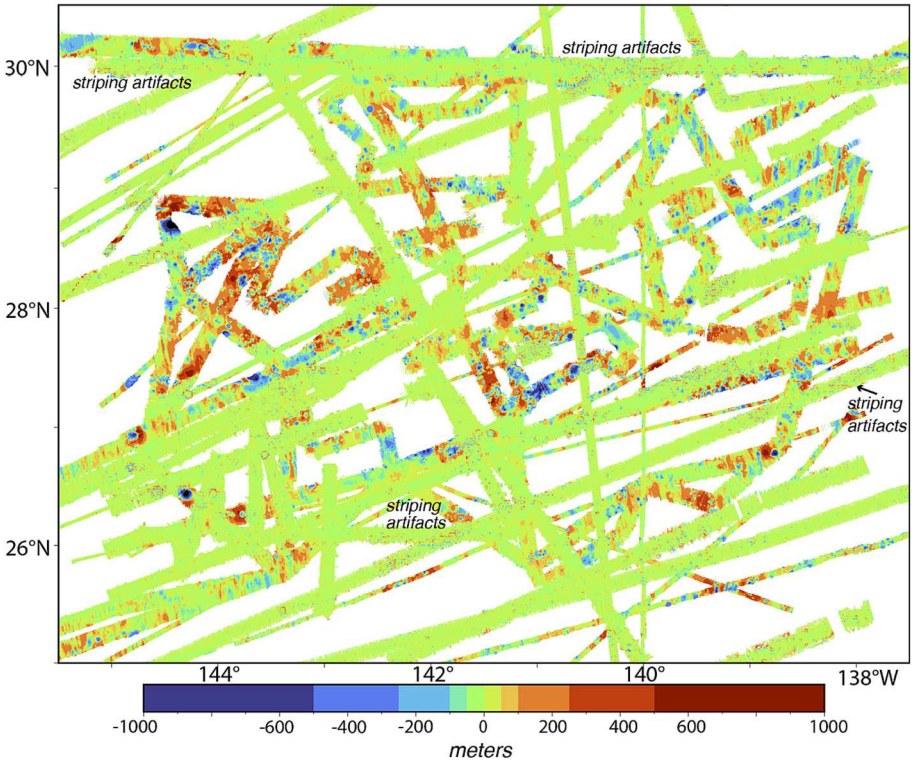

Fig. 4. Difference between measured seafloor depth and satellite gravity-based bathymetry model (SRTM15_V2.4 updated from Tozer et al., 2019), both gridded at 200 m interval.

contribution of seafloor topography, a reference constant crust model, and a local best-fit model of lithospheric cooling. The resulting residual anomaly map highlights deviations from this reference model.

4.1. Gravity processing method

The study area portion of the global satellite gravity grid (grav_32.1.nc, Sandwell et al., 2014) was used for the Free Air Anomaly (FAA). This 1-min resolution grid provides better coverage of our 500 × 600 km region than the available shipboard gravity data, which exist for notably fewer tracks than the MB data at the NCEI.

The contribution of seafloor topography to the FAA is predicted using the method of Parker (1973). Since a continuous 2-D interface is required by the method, we create a new 200 m grid with MB values wherever they exist and use the satellite-based model (Smith and Sandwell, 1997, updated in the SRTM15_V2.4 15′ grid) elsewhere. We only consider the Bouguer and residual gravity signals where there are MB data, so there is no circularity in using the gravity-based bathymetry model to fill in the MB gaps for this step. The interface is assumed to vary about the mean seafloor depth (4838 m), which is the distance that the signal is upward continued. The crustal layers are assumed to mimic the seafloor, with base at a subseafloor depth of 6 km, 1.5 km thick upper crust of density 2700 kg/m^3, and a 4.5 km thick lower crust of 2950 kg/m^3 (Sparks et al., 1980; Carlson and Raskin, 1984; Sinton and Detrick, 1992). The underlying mantle density is assumed to be 3300 kg/m^3. This results in density contrasts at the seafloor, upper/lower crust, and the crust/mantle interfaces of 1700, 250, and 350 kg/m^3, respectively. The bathymetry grid is mirrored in both directions (latitude and longitude) to avoid bias that would be introduced by an assumed periodically repeating, unmirrored edge (e.g. Blackman and Forsyth, 1991). Terms up to the 5th power in the series approximation are included. The seafloor, upper/lower crust, and crust/mantle interface contributions are summed and Fig. 5 compares this prediction to the satellite gravity map.

The seafloor + crust prediction is dominated by a decrease in values with plate age (Fig. 5b). This reflects the deepening of the ocean-crust interface for the older portion of the plate. However, the observed FAA (Fig. 5a and c) shows the opposite, with values generally ~10 mGal greater at 52 versus 40 Myr plate age. Cooling with distance from the oceanic spreading center results in thickening/densification of oceanic lithosphere and in the 40–52 Myr age bracket both a square-root of age and an exponential model fit the overall trend reasonably. Here we adopt Stein and Stein (1992) > 20 Myr exponential model and determine the best fit for our study area (Fig. 5a). Observed FAA values were shifted by +20 mGals and an exponential fit was obtained with Matlab curve fitting algorithm, ignoring (offset) values >36 mGal (16 mGal actual, Fig. 5a). Based on the Seton et al. (2020) age grid, we added to the seafloor + crust prediction the gravity increase with age:

$grav_{cool} = 3.0 \times \exp.(0.039 \times \text{age (Myr)})$ mGal.

The final step is to subtract the combined seafloor + crust + plate cooling predictions from the satellite FAA. The result is our residual gravity anomaly map (Fig. 6) where positive values indicate greater density, possibly thinner crust, than our reference model would predict. Negative values indicate lower density, possibly thicker crust or less dense mantle.

4.2. Relationship between residual gravity anomalies, segmentation, and bathymetric features

Much of the study area, particularly the central region, shows residual anomalies within 5 mGal of zero (Fig. 6), indicating that the reference model with constant crust and plate cooling/densification with age describes the subseafloor structure in general. Broad regions of excess mass occur in the western N and S corners, spanning several Myr of plate age and roughly coinciding with where second-order spreading segments either existed (SW) or developed (NW). Mass deficit occurs throughout the NE corner, increasing in magnitude as plate age decreases from ~43 to 40 Ma. All VR show mass deficit, with the two largest volcanic centers (~27°30′N, 141°W and 28°45′N, 144°30′W) reaching peak residual anomalies of 30–40 mGal. The negative anomalies associated with the smaller VR west of 143°30′W are lower at 10–12 mGal, with one central peak having a 20 mGal low. In this same western section, the moderate seamounts of >12 km diameter correspond to mass deficit of ~10 mGal whereas moderate seamounts elsewhere show ~5 mGal, residual anomaly. The fields of small volcanoes do not show any correlation with residual gravity anomaly. The two regions where abyssal hill trends consistently deviate from isochron-parallel do not share a relation to residual anomaly. The northeastern area is wholly within a mass deficit area but the deficit area extends well beyond where the abyssal hill trend deviates from the regional trend. The southeastern area of abyssal hill trend deviation has little or no mass anomaly relative to the reference model.

A likely explanation of VR mass deficit is that the crust is locally thicker, potentially including more porous volcanics within the shallow edifice as well as lower crust displacing mantle to flatten the base of the crust (the reference model has crust/mantle interface that shoals at the VR in concert with the seafloor). Estimates of the possible local crustal variation at VRs are obtained based on analytic expressions for a buried cylinder (e.g. Turcotte and Schubert, 1982) for scenarios of more porous, less dense volcanic edifice as well as for thickened lower crust. The sensitivity of these estimates was checked using a range of crustal density assumptions: 2300–2730 kg/m^3 for upper crust; 2850–2950 kg/m^3 for lower crust.

If most of the volcanic edifice has density of 2300–2400 kg/m^3 this could explain 18–25 mGal of the low anomaly. This density is in line with values assumed by Briais et al. (2009) in their analysis of volcano gravity signatures on the flank of the Pacific-Antarctic ridge. It is also in line with densities documented by drilling into Brothers Arc volcano, but only for the upper few hundred meters (Massiot et al., 2022). If most of the volcanic pile is not lower in density than ~2700 kg/m^3, lower crustal thickening of 2.5–3 km could generate the observed VR peak anomalies. The 3-km excess crustal thickness estimate corresponds to the topographic summit of the central VRs, where the lowest residual anomaly was determined (−40 mGal). The shoulders of these VR and all of the other VR are estimated to have up to 2–2.5 km excess crustal thickness, depending on their crustal and volcanic edifice densities. This would mainly serve to flatten the crust/mantle interface, relative to the reference model, although a modest crustal root is predicted for VR shallower than 2 km.

The broad NW mass excess occurs N of where an offset in the paleospreading center developed after 48 Ma, so it could reflect reduced magma supply for the prior several Myr (thinner crust) along that portion of the segment. In this scenario, the melt supply in the northern part of the spreading corridor begins to migrate E and the newly offset N segment tracks the melt supply in that direction, producing more typical crustal thickness for at least a couple Myr (our coverage of this segment is poor after 44 Ma). For the SW mass excess, this type of explanation may also apply. A 30 km offset in the ridge axis existed at the N edge of the mass excess area prior to 52 Ma. The offset decreased until it was eliminated by 48.5 Ma and the mass excess occurs only to the W of the 49 Ma isochron; its N boundary shifts to the S from 51.5 to 48.5 Ma. Possibly, lower melt supply (thinner crust) in the southern spreading segment was overtaken by an extending main segment where magma supply was more robust. The swath where residual depth that is 200–300 m shallower than the surrounding seafloor, stretching from OBS station P17, through P09, to N of P19 (Fig. 3), is not associated with a residual gravity anomaly. If thicker crust does support this broad swath of somewhat shallower seafloor, its density must be slightly greater than the crust to the N and S. It may be relevant that the region of mass excess in the SW tends to abut the southern boundary of this swath of shallower seafloor.

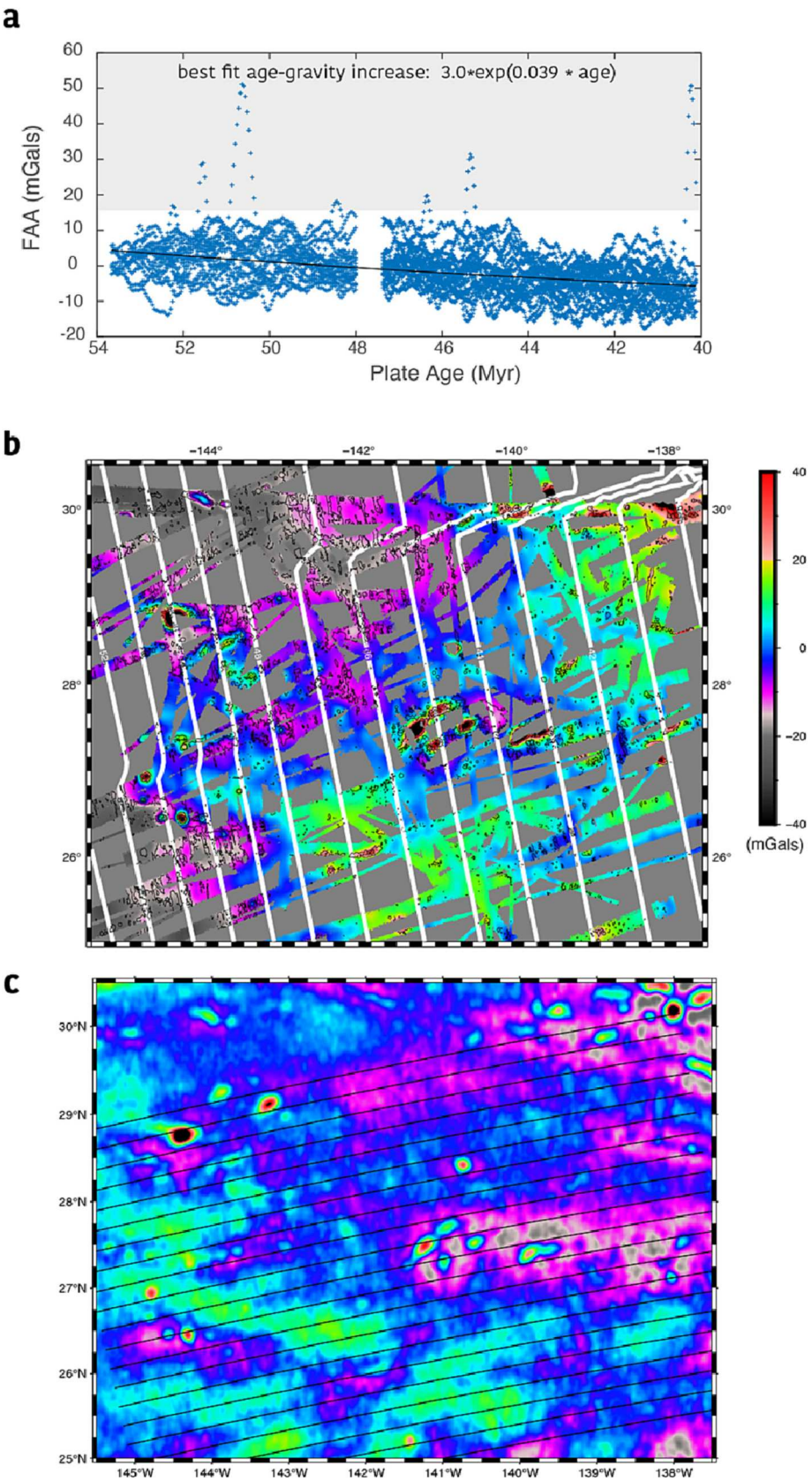

Fig. 5. Free Air gravity anomaly maps and profiles in the study area. a) Values of satellite Free Air Anomaly (FAA) along spreading-parallel transects (thin black lines in c) plotted as a function of plate age. Change in spreading rate at 48 Ma is plotted as if instantaneous (gap). Black line shows exponential fit. b) Map of predicted seafloor plus constant crust contribution to FAA. White contours show plate age (Myr; Seton et al., 2020). c) Satellite FAA map (Sandwell et al., 2014).

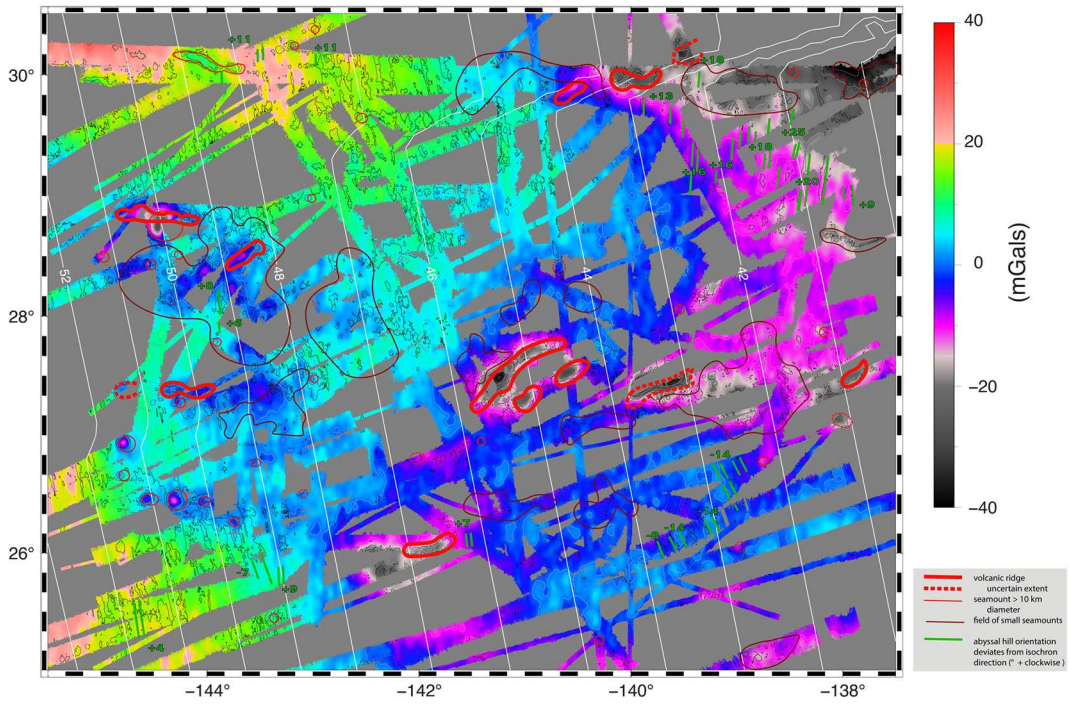

Fig. 6. *(below)*. Residual gravity anomaly. Volcanic features are shown (legend, lower right). Thick white lines show plate age (Myr). Thin black contours mark residual bathymetry >4500 m depth at 500 m interval. Thin white contours are every 10 mGal.

5. Discussion

The distribution of seafloor volcanism in our study area indicates that magma was supplied outside of the upwelling zone where partial melting was active along the spreading center (now subducted) that created this portion of the Pacific plate. Some of this volcanic activity probably reflects incomplete channeling of melt from the broad upwelling zone to the spreading axis, but the larger volcanic features were probably fed by a separate melt source, after the ridge flank had aged at least several Myr, as discussed below.

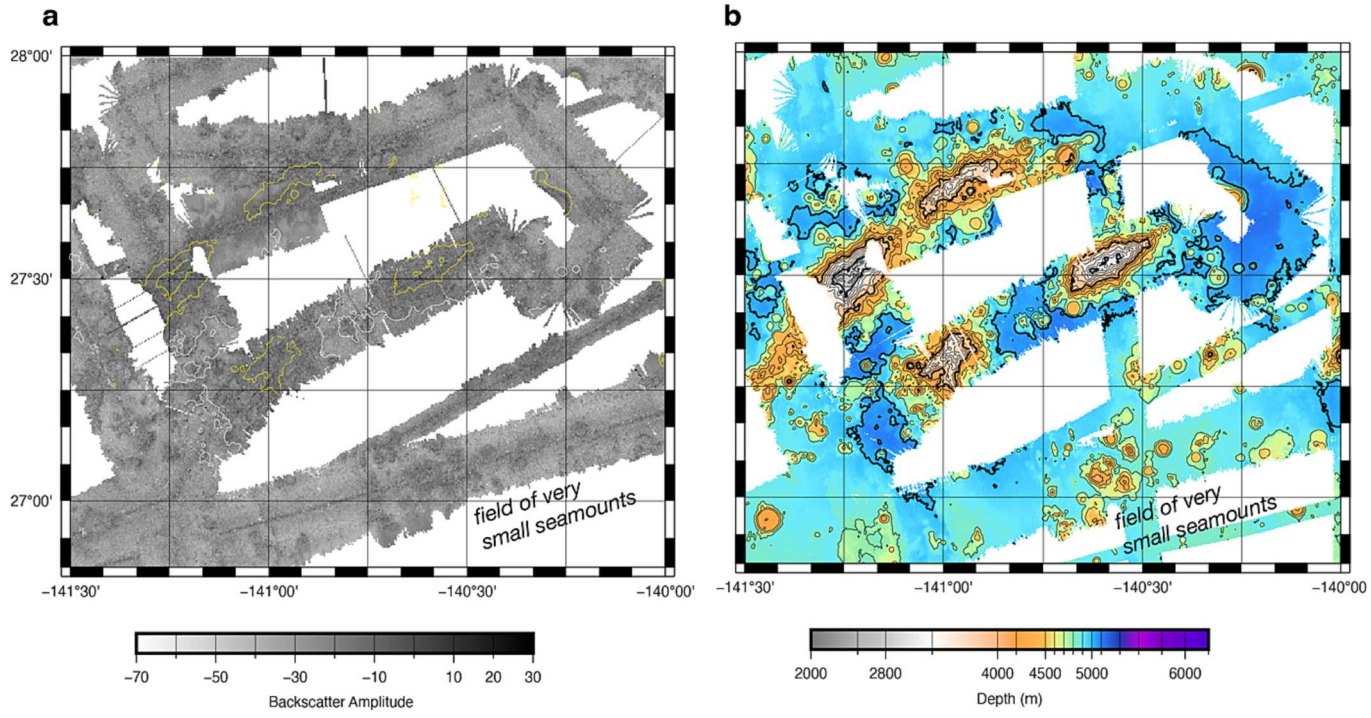

Fig. 7. Example of Volcanic Ridges (VR) and a field of very small seamounts. a) Backscatter image shows hummocky character of VR which lack central caldera. Dark shade indicates stronger acoustic returns from sloping/rough seafloor. Abyssal hill morphology is not evident. Selected 1000-m-interval contours outline VR and nearby smaller seamounts: yellow ≤4000 m; white = 5000 m. b) Bathymetric map of the same area, contoured at 200 m interval. (For interpretation of the references to color in this figure legend, the reader is referred to the web version of this article.)

The fact that the fields of very small seamounts do not display an abyssal hill fabric probably indicates that these formed within 5–15 km of the paleo axis, with local magma injection relieving stress that otherwise would have contributed to faulting that could accommodate uplift and rotation of back-tilted abyssal hill blocks (Macdonald et al., 1996; Fig. 7).

While the height of some of the very small seamounts in the fields do exceed typical abyssal hill height, both the bathymetry and sidescan data suggest that outflow beyond their local edifices was not great enough to bury adjacent abyssal hill scarps, if they'd existed. This supports our inference that stress relief associated with near-axis magma supply inhibited faulting and abyssal hill formation. These very small seamount eruptions onto ridge flank that was probably <0.2 Myr old likely indicate diversion of melt from the main subaxial supply. Prior studies with more complete coverage, samples, and age dating of young ridge flank volcanism (Briais et al., 2009; Alexander et al., 1996; Shen et al., 1993; White et al., 1998) show that most small-moderate sized seamounts form within ~15 km of the axis. However, those areas (Pacific-Antarctic ridge 40°-50°S, EPR 9–10° N and 15°-20° S, respectively) commonly display clear abyssal hill fabric adjacent to the small seamounts, contrary to what we observe.

The moderate seamounts are not cut by faults, which suggests they either formed after the plate was ~0.8 Myr old, after which abyssal hill formation on the EPR has been shown to cease (Crowder and Macdonald, 2000), or that the volcanic effusion was sufficient to continously fill developing grabens and cover scarps. The line of moderate seamounts in the NW of the study area is surrounded by abyssal hill fabric (Figs. 3 and 8). This doesnt constrain the timing of volcanic activity but the structure is similar to that observed at the west end of the North Menard volcanic ridge (Briais et al., 2009). Age dating of basalt samples by those authors indicate that North Menard chain formed on ~1.5 Myr old ridge flank.

The Volcanic Ridges extend across a 0.3–2 Myr plate age range and their likely thicker crust (negative residual gravity anomaly) indicates notable magma supply. The lack of a moat around these VR (Figs. 3 and 7) indicates that the plate onto which they erupted was strong (thick) enough to support km-scale loads, and this indicates they formed when the plate was several Myr old or more. Sediment accumulation in this area is low and the character of the seafloor adjacent to the VR does not indicate thick sediment ponding that would obscure a moat. We do not have any age information for the VR, but their morphology, roughly central peak (negative) residual gravity anomaly, and the fact that they do not trace the direction of absolute plate motion suggest they are not age progressive. Other (longer) linear volcanic features in the Pacific are known not to be age progressive (e.g. Forsyth et al., 2006; Fabrizzi et al., 2023).

We cannot rule out low density in the mantle below the VR as a contributing factor of their residual gravity anomalies. Basaltic melt pockets or channels, either currently molten or crystallized (gabbro), within peridotite would reduce the local mass relative to surrounding mantle host rock. To produce a signal no wider than the width of the VR and up to several tens mGal in amplitude (the full amplitude observed so a maximum estimate), a zone on the order of 6 km wide with up to 50% basalt/gabbro would be required, based on simple estimates for a buried cylinder (e.g. Turcotte and Schubert, 1982). If this amount of melt were currently present, geologically recent eruptions might be expected to result in fresh lava on the seafloor. The sidescan sonar data (Figs. S2 and 7) do not show the strong reflectivity characteristic of fresh rock. Instead, the signature is more typical of hummocky relief where slope contributes to somewhat increased backscatter, relative to surroundings, rather than the nature of the material at the seafloor. Thus, we prefer the interpretation of thickened crust, possibly with shallow lower density due to greater porosity, along the VR rather than present-day melt in the mantle. Regardless, the seismic structure of the crust and possibly the underlying mantle will likely have been altered as magma was supplied off-axis from depth, pooled for some time in magma chamber(s), and made its way through fracture (networks) toward the seafloor.

North of the study area, a series of seamounts known as the Moonless Mountains extends along ~31°N latitude between 143°W and 137°W (Fig. 9). Their summits are generally 1000 m shallower than the VR in our study area, based on data available in the Global Multi-Resolution

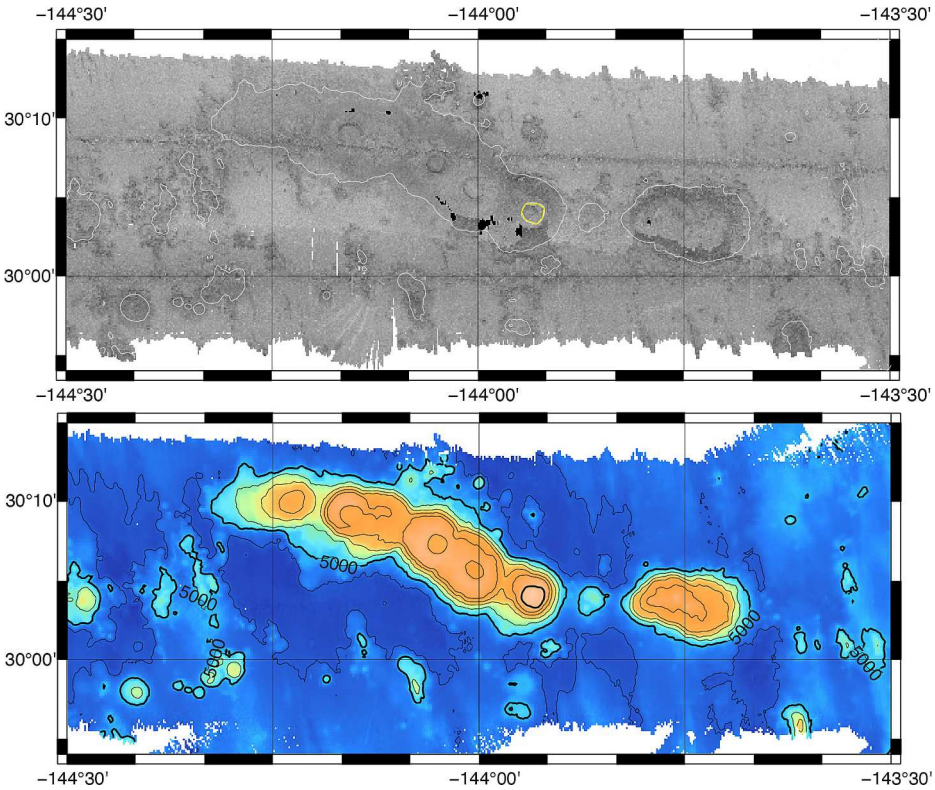

Fig. 8. Line of moderate seamounts in NW of study area. Backscatter (upper) and bathymetry (lower) shade/color scales and contour intervals are the same as Fig. 7.

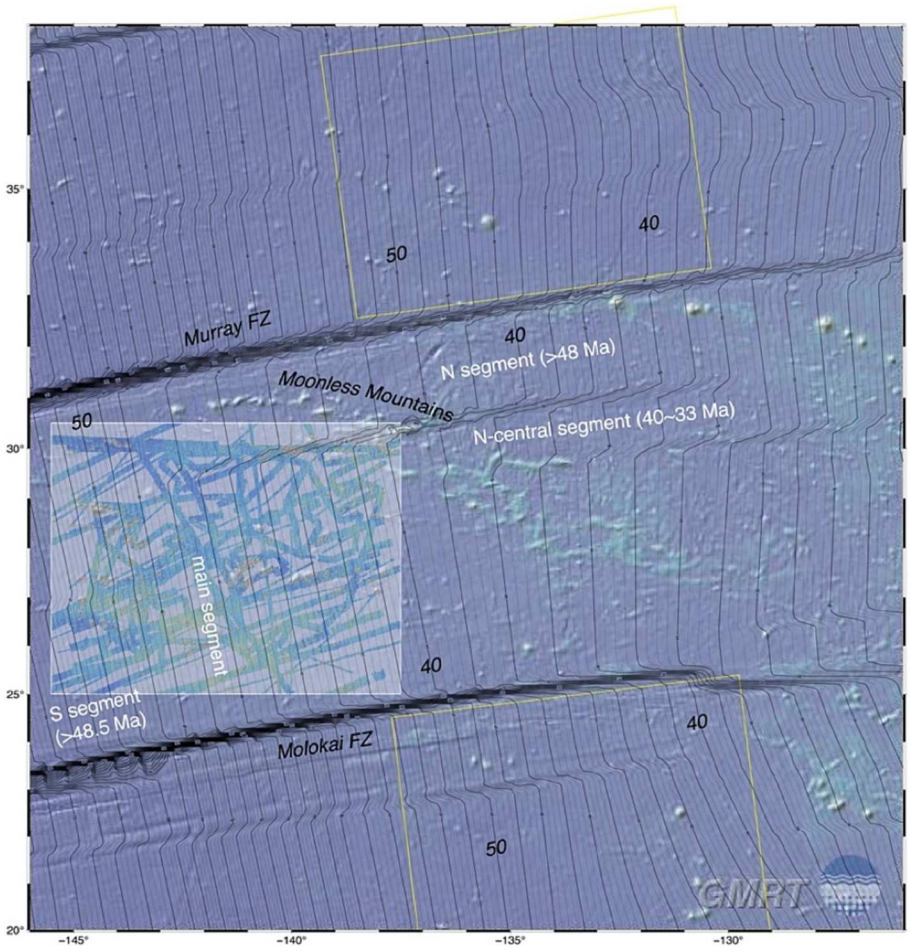

Fig. 9. Bathymetry, isochrons (Myr; Seton et al., 2020), and segmentation within and either side of the study area (box with MB data overlain on GMRT map). Yellow boxes outline crust of the same age to the N and S of the bounding Fracture Zones (FZ). (For interpretation of the references to color in this figure legend, the reader is referred to the web version of this article.)

Topography synthesis (GMRT, Ryan et al., 2009). However, a few of the smaller, more linear features in Moonless Mountains are similar in height and trend to the VR observed in our area.

Smith and Jordan (1988) previously noted that the density of seamounts changes across some Pacific fracture zones. Their sparse coverage showed a significantly lower density of seamounts north of the Molokai-Murray FZs corridor. Our increased coverage in the 40–52 Ma portion of the plate shows the corridor has experienced notable off-axis volcanic activity. Comparison of seamount distributions on 40–52 Ma crust north of the Murray FZ and south of the Molokai FZ (Fig. 9, using GMRT) shows that elongate VR do not occur either side of our spreading corridor. Moderate seamount numbers appear to be similar for these plate ages between the areas but MB coverage in the area S of Molokai FZ is quite sparse (Fig. 4 shows that satellite-derived bathymetry can misrepresent these features). Carbotte et al. (2004) find that, along the N EPR, spreading segments that 'lead' plate boundary migration over the deep mantle have more robust magma supply, resulting in shallower seafloor, possibly thicker crust. The Molokai-Murray corridor would be predicted to follow this pattern with its large westward lead. Certainly more magmatic activity has occurred here but there is no clear pattern of shallow seafloor or thick crust, the latter inferred from (non-unique) gravity interpretation. The majority of the excess magma was erupted at the VR which we infer to have formed only after the plate was well outside the axial upwelling/partial melting zone (> several Myr old), beyond where Carbotte's hypothesis of lithospheric slope channeling should come into play. We do observe that more of the 40–52 Ma seafloor has fields of very small seamounts than elsewhere and this could reflect near-axis difference in melt delivery. Without actual dates for the VR, further assessment of the possible melt source and its relation to past axial upwelling zone is premature, but detailed comparison including seismic constraints would allow Carbotte et al. (2004) hypothesis to be tested in this region. The volcanic features in this corridor do not display a relationship between the location of ridge offsets and the occurence of off-axis magmatism (Fig. 9), as had been determined by Gomez and Briais (2000) to characterize other sections of the EPR and Pacific-Antarctic ridge.

We can compare our findings with that of other recent OBS array studies in the Pacific, where MB data coverage in remote parts of the basin at 500 km extent are along the lines of our study, so inferences can be made with confidence. The ORCA experiment (Eilon et al., 2022) included an area around 40 Myr old lithosphere in the central Pacific, N of Marquesas FZ, 4–8°S. These MB data are included in GMRT. Coverage is more sparse than for our study area but, where MB data exist, ORCA seafloor displays abyssal hill fabric throughout. About a dozen moderate seamounts occur along with several isolated very small seamounts. No VR occur and only a single ~50 km wide field of more densely spaced very small seamounts. The NoMELT magnetotelluric and OBS arrays covered a similar sized area centered on 70 Myr old Pacific lithosphere SE of the Hawaiian chain (Sarafian et al., 2015; Russel et al., 2022). The MB data from those deployment and recovery cruises, along with a few other tracks in the area that are also included in GMRT, again display abyssal hill fabric throughout the region. There are 3–4 times as many moderate seamounts as in the ORCA area, and their spatial density is about twice as high as in our study area. However, there are no VR and

no fields of very small seamounts. Overall, the character of the NoMELT seafloor is most similar to the SW portion of our study area, where abyssal hills are dominant and the density of moderate seamounts is greatest.

Neither our study area nor the ORCA or NoMELT areas show any pattern of seamount abundance with plate age. While some early studies (Batiza, 1982; Smith and Jordan, 1988) estimated from sparse data that the number of seamounts increased with plate age across the Pacific, more complete data and analysis led Hillier and Watts (2007) to conclude that spreading segment axial conditions at the time of plate accretion was likely the dominant control on the distribution of seamount formation. Our residual gravity anomaly map along with the lack of a strong morphological pattern within our study area support the Hillier and Watts interpretation.

6. Conclusions

New mapping, compiled with pre-existing multibeam sonar data, enable a detailed characterization of 40–52 Myr old Pacific seafloor in the spreading corridor between the Molokai and Murray fracture zones. As expected, a reference model of constant thickness, constant density crust, and lithosphere cooling and deepening in proportion to plate age can explain the broad structure of the area, but residual features also stand out. Spreading-center parallel abyssal hills are dominant in about 60% of the study area but are not evident in most areas where volcanic features exist. Volcanic ridges, 30–120 km in length and 1–2 km high, and moderate seamounts, with diameter 8–15 km and several 100's m height, cover several percent of the seafloor. While this percentage is in line with prior studies of volcano distribution in the Pacific, an additional ~25% of our study area is covered by fields of greater than typical density of very small seamounts. Gravity analysis suggests that crustal variability can explain the seafloor features that we describe. Much of the variation in volcanism was likely related to evolving spreading segment magmatic conditions early in the formation of the plate, including lengthening and elimination of ridge offsets and magma migrating to the seafloor outside the main rift but within 10–15 km of the axis. The volcanic ridges were likely active only after the plate was at least several Myr old, indicating a separate (non spreading) source of magma.

CRediT authorship contribution statement

Donna K. Blackman: Conceptualization, Data curation, Formal analysis, Funding acquisition, Investigation, Methodology, Software, Supervision, Validation, Visualization, Writing – original draft. **Sujania Talavera-Soza:** Formal analysis, Writing – review & editing. **Ruei-Jiun Hung:** Formal analysis, Writing – review & editing. **John A. Collins:** Funding acquisition, Investigation, Writing – review & editing. **Gabi Laske:** Funding acquisition, Project administration, Writing – review & editing.

Declaration of competing interest

The authors declare the following financial interests/personal relationships which may be considered as potential competing interests.

Donna Blackman reports financial support was provided by U.S. National Science Foundation.

Data availability

The edited MB swath data, both new and pre-existing are archived at the US Marine Geoscience Data System (MGDS). The 200 m bathymetry grid and the corresponding residual gravity anomaly grid are also archived at the MGDS *(DOIs:* 10.26022/IEDA/331356 and 10.26022/IEDA/331358, respectively*)* and are freely available for immediate download and use

Acknowledgements

This work was supported by the National Science Foundation OCE-1830959; dkb also received minor support from NASA grant 80NSSC19K1427 for an aspect of this work. We thank the crews of *R/V Kilo Moana* and *R/V Sally Ride* for their support in acquiring the new multibeam sonar data. We appreciate the extra effort, associated with conducting marine operations during the Covid-19 pandemic, by personnel at the Marine Facilities of University of Hawaii, Scripps Institution of Oceanography, and the Integrated Programs Section at NSF Ocean Sciences division. We appreciate comments by Scott White and 2 anonymous reviewers, which helped improve the manuscript.

References

Alexander, R.T., Macdonald, K.C., 1996. Small off-axis volcanoes on the East Pacific rise. EPSL 139, 387–394.

Atwater, T., 1989. Plate tectonic history of the Northeast Pacific and western North America. In: Winterer, E.L., Hussong, D.M., Decker, R.W. (Eds.), The Eastern Pacific and Hawaii, Boulder CO, Geological Society of America. The Geology of North America, V. N.

Batiza, R., 1982. Abundances, distribution and sizes of volcanoes in the Pacific Ocean and implications for the origin of non-hotspot volcanoes. Earth Planet. Sci. Lett. 60 https://doi.org/10.1016/0012-821X(82)90003-6.

Blackman, D.K., Forsyth, D.W., 1991. Isostatic compensation of tectonic features of the Mid- Atlantic Ridge: 25-27°S. J. Geophys. Res. 96 https://doi.org/10.1029/91jb00602.

Briais, A., Ondréas, H., Klingelhoefer, F., Dosso, L., Hamelin, C., Guillou, H., 2009. Origin of volcanism on the flanks of the Pacific-Antarctic ridge between 41°30'S and 52°S. Geochem. Geophys. Geosyst. 10 https://doi.org/10.1029/2008GC002350.

Carbotte, S.M., Small, C., Donnelly, K., 2004. The influence of ridge migration on the magmatic segmentation of mid-ocean ridges. Nature 429, 743–746.

Carlson, R.L., Raskin, G.S., 1984. Density of ocean crust. Nature 311, 555–558.

Crowder, L.K., Macdonald, K.C., 2000. New constraints on the width of the zone of active faulting on the East Pacific rise 8°30'N-10°N from SeaBeam bathymetry and SeaMARCII side-scan sonar. Mar. Geophys. Res. 21 https://doi.org/10.1023/A:1004875609890.

Eilon, Z.C., Gaherty, J.B., Zhang, L., Russell, J., McPeak, S., Phillips, J., Forsytg, D.W., Ekstrom, G., 2022. The Pacific OBS Research into Convecting Asthenospher (ORCA) Experiment. Seismol. Res. Lett. 93 https://doi.org/10.1785/0220210173.

Fabrizzi, A., Parnell-Turner, R., Gregg, P.M., Fornari, D.J., Perfit, M.R., Wanless, V.D., Anderson, M., 2023. Relative timing of off-axis volcanism from sediment thickness estimates on the 8°20'N seamount chain. East Pacific Rise, GCubed. https://doi.org/10.1029/2022GC010335.

Forsyth, D.W., Harmon, N., Scheirer, D.S., Duncan, R.A., 2006. Distribution of recent volcanism and the morphology of seamounts and ridges in the GLIMPSE study area: Implications for the lithospheric cracking hypothesis for the origin of intraplate, non–hot spot volcanic chains. J. Geophys. Res. 111, B11407. https://doi.org/10.1029/2005JB004075.

Fox, P.J., Gallo, D., 1984. A tectonic model for ridge-transform-ridge plate boundaries: Implications for the structure of oceanic lithosphere. Tectonophys. 104 https://doi.org/10.1016/0040-1951(84)90124-0.

Gee, J.S., Kent, D.V., 2007. Source of oceanic magnetic anomalies and the geomagnetic polarity timescale. Treat. Geophysics, Chapter 5 (12), 455–507. https://doi.org/10.1016/B978-044452748-6.00097-3.

Gomez, O., Briais, A., 2000. Near-axis seamount distribution and its relationship with the segmentation of the East Pacific rise and northern Pacific-Antarctic ridge, 17°N-56°S. Earth Planet. Sci. Lett. 175, 233–246.

Harrison, C.G.A., Sclater, J.G., 1972. Origin of the disturbed magnetic zone between the Murray and Molokai fracture zones. Earth Planet. Sci. Lett. 14, 419–427.

Hillier, J.K., Watts, A.B., 2007. Global distribution of seamounts from ship-track bathymetry data. Geophys. Res. Lett. 34, L13304. https://doi.org/10.1029/2007GL029874.

Key, K., Constable, S., Liu, L., Pommier, A., 2013. Electrical image of passive mantle upwelling beneath the northern East Pacific rise. Nature 495. https://doi.org/10.1038/nature11932.

Laske, G., Collins, J., Blackman, D., 2023. The OHANA OBS Deployment in the Northeast Pacific Ocean. In: IUGG abstract JS03, p. 258.

Macdonald, K.C., 1982. Mid-ocean ridges: Fine scale tectonic, volcanic and hydrothermal processes within the plate boundary zone. Annu. Rev. Earth Planet. Sci. 10 https://doi.org/10.1146/annurev.ea.10.050182.001103.

Macdonald, K.C., Fox, P.J., Alexander, R.T., Pocklany, R., Gente, P., 1996. Volcanic growth faults and the origin of Pacific abyssal hills. Nature 380, 125–129.

Massiot, C., McIntosh, I., Deans, J., Milicich, S.D., Caratori Tontini, F., de Ronde, C.E.J., Adam, L., Kolandaivelu, K., Guerin, G., 2022. Petrophysical Facies and Inferences on Permeability at Brothers Volcano, Kermadec Arc, Using Downhole Images and Petrophysical Data. Economic Geology. https://doi.org/10.5382/econgeo.4897.

Parker, R.L., 1973. The rapid calculation of potential anomalies. Geophys. J. R. Astron. Soc. 31, 447–455. https://doi.org/10.1111/j.1365-246X.1973.tb06513.x.

Parsons, B., Sclater, J.G., 1977. An analysis of the variation of ocean floor bathymetry and heat flow with age. J. Geophys. Res. 88 https://doi.org/10.1029/JB082i005p00803.

Russel, J.B., Gaherty, J.B., Mark, H.F., Hirth, G., Hansen, L.N., Lizaralde, D., Collins, J.A., Evans, R.L., 2022. Seismological evidence for girdled olivine lattice-preferred orientation in the oceanic lithosphere and implications for mantle deformation processes during seafloor spreading. Geochem. Geophys. Geosyst. 23 https://doi.org/10.1029/2022GC010542.

Ryan, W.B.F., Carbotte, S.M., Coplan, J., O'Hara, S., Melkonian, A., Arko, R., Weissel, R. A., Ferrini, V., Goodwillie, A., Nitsche, F., Bonczkowski, J., Zemsky, R., 2009. Global Multi-Resolution Topography (GMRT) synthesis data set. Geochem. Geophys. Geosyst. 10, Q03014. https://doi.org/10.1029/2008GC002332.

Sandwell, D.T., Müller, R.D., Smith, W.H.F., Garcia, E., Francis, R., 2014. New global marine gravity model from CryoSat-2 and Jason-1 reveals buried tectonic structure. Science 346 (6205), 65–67. https://doi.org/10.1126/science.1258213.

Sarafian, E., Evans, R.L., Collins, J.A., Elsenbeck, J., Gaetani, G.A., Gaherty, J.B., Hirth, G., Lizaralde, D., 2015. Geochem. Geophys. Geosyst. 16 https://doi.org/10.1002/2014GC005709.

Seton, M., Müller, R.D., Zahirovic, S., Williams, S., Wright, N.M., Cannon, J., et al., 2020. A global data set of present-day oceanic crustal age and seafloor spreading parameters. Geochem. Geophys. Geosyst. 21 https://doi.org/10.1029/2020GC009214 e2020GC009214.

Shen, Y., Forsyth, D.W., Scheirer, D.S., Macdonald, K.C., 1993. Two forms of volcanism: implications for mantle flow and off-axis crustal production on the west flank of the southern East Pacific rise. J. Geophys. Res. 98 https://doi.org/10.1029/93JB01721.

Sinton, J.M., Detrick, R.S., 1992. Mid-ocean ridge magma chambers. J. Geophys. Res. 97 https://doi.org/10.1029/91JB02508.

Smith, D.K., Jordan, T.H., 1988. Seamount statistics in the Pacific Ocean. J. Geophys. Res. 93 https://doi.org/10.1029/JB093iB04p02899.

Smith, W.H.F., Sandwell, D.T., 1997. Global seafloor topography from satellite altimetry and ship depth soundings. Science 277, 1957–1962.

Sparks, D.W., Parmentier, E.M., 1992. Three-dimensional mantle convection beneath a segmented spreading center: Implications for along-axis variations in crustal thickness and gravity. J. Geophys. Res. 98 https://doi.org/10.1029/93JB02397.

Sparks, R.S.J., Meyer, P., Sigurdsson, H., 1980. Density variation amongst mid-ocean ridge basalts: Implications for magma mixing and the scarcity of primitive lavas. Earth Planet. Sci. Lett. 46 https://doi.org/10.1016/0012-821X(80)90055-2.

Stein, C.A., Stein, S., 1992. A model for the global variation in oceanic depth and heat flow with lithospheric age. Nature 359, 123–129.

Tozer, B., Sandwell, D.T., Smith, W.H.F., Olson, C., Beale, J.R., Wessel, P., 2019. Global bathymetry and topgraphy at 15 Arc Sec: SRTM15+. Earth Space Sci. 6 https://doi.org/10.1029/2019EA000658.

Turcotte, D.L., Schubert, G., 1982. Geodynamics. Wiley and Sons, NY.

Wang, Y., Forsyth, D.W., Savage, B., 2009. Convective upwelling in the mantle beneath the Gulf of California. Nature 462. https://doi.org/10.1038/nature0852.

Wessel, P., Luis, J.F., Uieda, L., Scharroo, R., Wobbe, F., Smith, W.H.F., Tian, D., 2019. The Generic Mapping Tools version 6. Geochem. Geophys. Geosyst. 20 https://doi.org/10.1029/2019GC008515.

White, S.M., Macdonald, K.C., Scheirer, D.S., Cormier, M.-H., 1998. Distribution of isolated volcanoes on the flanks of the East Pacific rise. JGR 103, 30,371–30,384.